

## Nanogenerator as an active sensor for vortex capture and ambient wind-velocity detection†

Rui Zhang,<sup>ab</sup> Long Lin,<sup>a</sup> Qingshen Jing,<sup>ac</sup> Wenzhuo Wu,<sup>a</sup> Yan Zhang,<sup>a</sup> Zongxia Jiao,<sup>b</sup> Liang Yan,<sup>b</sup> Ray P. S. Han<sup>c</sup> and Zhong Lin Wang<sup>\*ad</sup>

Received 28th May 2012, Accepted 26th June 2012

DOI: 10.1039/c2ee22354f

In this paper, we report a simple and practical composite structure for a nanogenerator (NG). The composite design using two kinds of piezoelectric materials, zinc oxide and poly(vinylidene fluoride), requires no more system size and complexity than for a single material, but improves the power density and sensitivity of the NG significantly. With no need of an external power source or batteries, the composite NG can efficiently convert the vortex motion in the atmosphere into electricity. Based on the Karman vortex street principle, ambient wind-speed measurements with the NG are demonstrated. Due to the simple structure, high sensitivity and good environment-friendly properties, the NG as an active sensor should play an important role in wireless environmental monitoring networks.

### 1. Introduction

Self-powered nanosystem is a promising concept for the realization of environmental wireless sensor networks. Due to the enormous demands of distributed nodes in the networks, the disadvantages of conventional battery-based sensors, such as large package size, low device maintainability, high system cost and risk of environment pollution, are important issues.<sup>1–3</sup> Thus, a battery-free autonomous system that scavenges its operation energy from the surroundings is highly desired. Solar, thermal and mechanical (wind, water flow, vibration, friction and body movement) energies are common in the ambient environment. The type of energy to be scavenged depends on the specific application. Solar and thermal energies are time and location dependent, which are hard to be reached continuously. Mechanical energy is a potential solution for the independent, sustainable and wireless operation of self-powered wireless sensor networks. Since the first zinc oxide nanowire (ZnO NW) based piezoelectric nanogenerator (NG) was demonstrated in 2006,<sup>4</sup> various NGs have been developed for ultrasonic,<sup>5,6</sup> vibration,<sup>7–9</sup> air pressure<sup>10</sup> and body movement<sup>11</sup> energies harvesting. In addition to powering other devices, the electricity outputs of these NGs can also be analyzed to reveal the properties of their input motions. Some applications of NGs as active sensors for heart-pulse,<sup>10</sup> tire pressure<sup>12</sup> and cantilever vibration<sup>13</sup> measurements have been reported. Moreover, the feasibility of self-powered nanosystems utilizing NGs/active-sensors has been substantiated.<sup>14,15</sup> Until now, great efforts have been put into investigating the basic principle and structural design of

<sup>a</sup>School of Materials Science and Engineering, Georgia Institute of Technology, Atlanta, GA 30332, USA. E-mail: zhong.wang@mse.gatech.edu

<sup>b</sup>School of Automation Science and Electrical Engineering, Beihang University, Beijing, 100191, China

<sup>c</sup>College of Engineering, Peking University, Beijing, 100871, China

<sup>d</sup>Beijing Institute of Nanoenergy and Nanosystems, Chinese Academy of Sciences, Beijing, China

† Electronic supplementary information (ESI) available. See DOI: 10.1039/c2ee22354f

### Broader context

We present a simple and practical composite structure for a nanogenerator (NG) or active-sensor for mechanical energy harvesting and vortex-based gas/liquid flow measurements. The composite design uses two kinds of piezoelectric material, ZnO and poly(vinylidene fluoride) (PVDF). The power density and sensitivity of the composite NG are improved significantly. For energy recovery applications, the large electricity output of the NG results in a high working efficiency. Moreover, as an active nanosensor, the NG's high sensitivity and resolution makes it particularly suitable for detection of tiny deformations/mechanical-triggering. Utilizing the high performance NG, we demonstrate a simple and inexpensive method for flow measurement. As an active fluid sensor, the NG-based vortex flow device (VFD) is developed for tiny ambient wind detection. Experimental results show that the NG-based VFD has a low working limit of only 0.6 m s<sup>-1</sup>. While, commercial vortex flow meters for air generally work in the range from 6 m s<sup>-1</sup> to 80 m s<sup>-1</sup>.<sup>17</sup> Moreover, the NG-based active VFD has the advantages of high noise tolerance, long life time, low system cost and no environment pollution risk. It should play important roles in environment air/water flow detection and oil/gas pipeline monitoring.

NGs, active sensors and self-powered systems. However, to implement self-powered wireless sensor networks, more types of NGs/active-sensors are still urgently demanded to meet the diverse measurement requirements.

Herein, we present a simple and practical composite structure for a NG/active-sensor for ambient vortex-energy harvesting and gas-liquid flow measurement. The composite design consisting of two kinds of piezoelectric material, ZnO and poly(vinylidene fluoride) (PVDF), requires no more system size and complexity than conventional ZnO NGs. Meanwhile, the power density and sensitivity of the composite NG are improved significantly. For energy recovery applications, the large electricity output of the NG results in a high working efficiency. Moreover, as an active nanosensor, NG with high sensitivity and resolution is particularly suitable for detection of tiny deformation/mechanical-triggering.<sup>13,16</sup> Utilizing the high performance NG, we demonstrate a simple and inexpensive method for vortex capture and flow measurement. As an active fluid sensor, a NG-based vortex flow device (VFD) is developed for tiny ambient wind detection. Experimental results show that the NG-based VFD has a lower working limit of only  $0.6 \text{ m s}^{-1}$ . While, a commercial vortex flow meter for air generally works in the range from  $6 \text{ m s}^{-1}$  to

$80 \text{ m s}^{-1}$ .<sup>17</sup> Moreover, the NG-based active VFD has the advantages of high noise tolerance, long life time, low system cost and no environment pollution risk. It should play an important role in environmental air/water flow detection and oil/gas pipeline monitoring.

## 2. ZnO&PVDF composite NG

The NG is one of the most important components in self-powered systems and active sensors. To achieve high power output and high sensitivity of the NG, we propose a composite structure as shown in Fig. 1a. It has a laminated structure, including a bottom Ag electrode, a PVDF film (Measurement Specialties Inc.,  $28 \mu\text{m}$  in thickness), an ITO adhesion layer, a ZnO seed layer, a ZnO NW array, a poly(methyl methacrylate) (PMMA) (MicroChem, 950 PMMA A11) insulation layer and a top Ag electrode. The ZnO seed layer is to assist the compact growth of ZnO NWs using a hydrothermal method.<sup>14,18</sup> Fig. 1c and d are scanning electron microscopy (SEM) images of the as-grown ZnO NWs. The oblique view in Fig. 1c shows that the ZnO NWs are grown tightly on the PVDF film through the ITO adhesion layer and the ZnO seed layer. The inset of Fig. 1c is a cross-sectional view, which indicates that the length of the ZnO NWs

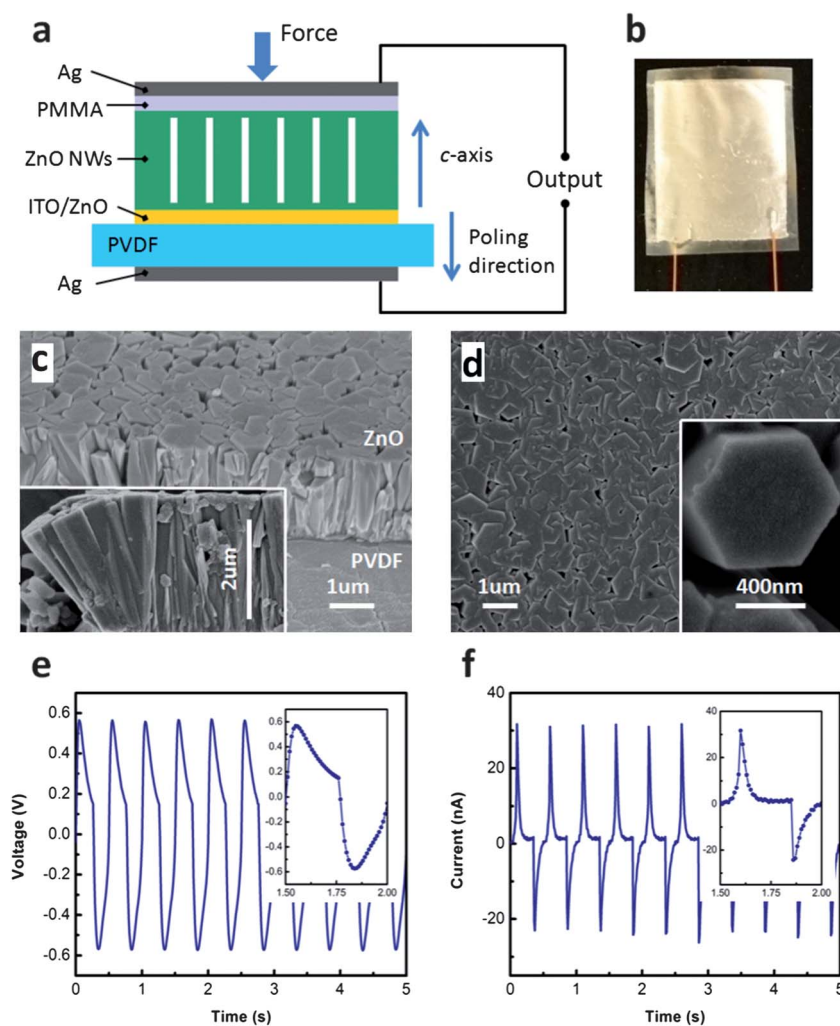


**Fig. 1** Design, characterization and test of NG. (a) Schematic diagram of the NG. (b) Photo of the NG. (c) SEM images of a ZnO NWs array grown on a PVDF substrate. The inset shows a magnified cross-sectional image. (d) Top-view of the ZnO NWs array. The inset shows a magnified image of a ZnO NW. Electrical characteristics of the NG. (e) Voltage output. (f) Current output.

is about 2.8  $\mu\text{m}$ . From the top view in Fig. 1d, we can see that the ZnO NWs are grown densely to form a uniform film. A magnified ZnO NW in the inset of Fig. 1d shows that the NW is about 800 nm in diameter. According to the growth mechanism of ZnO NWs,<sup>18</sup> the *c*-axis of these NWs is their growth direction, which is parallel to the poling direction of the PVDF film. The PVDF film plays two important roles in this structure. On one hand, it works as a substrate supporting the whole structure. The utilization of the PVDF film in the composite structure requires no more processing than conventional ZnO NGs. With a flexible PVDF substrate, the NG can be easily tailored for specific applications. On the other hand, it is known that the piezoelectric coefficient of PVDF is negative, while that of ZnO NWs is positive.<sup>19</sup> Thus, by arranging the materials so that the direction of the *c*-axis of the ZnO NWs is opposite to the poling direction of the PVDF film, the piezoelectric potentials in these two materials add up when the composite structure is pressed. The piezoelectric potentials lead to an electric potential difference across the top and bottom Ag electrodes. For electricity output, leads are

connected to the top and bottom electrodes. Fig. 1b shows the NG with a dimension of 15 mm  $\times$  18 mm and an effective region of 12 mm  $\times$  15 mm. The electrical output of the NG is investigated using a linear motion stage shown in Fig. S1d (ESI<sup>†</sup>). A linear motor (Labworks Inc., ET-132-203) moves up and down to strike the NG periodically. To apply a uniform pressure, the NG is sandwiched between a glass substrate and a small glass cover (12.5 mm  $\times$  25.4 mm). The NG is struck with a peak stress of  $6.1 \times 10^4$  Pa at 2 Hz frequency, and its electrical outputs are shown in Fig. 1e and f. The peak outputs of voltage and current are 0.57 V and 32 nA, respectively. For a comparison, experiments on other structures are implemented under the same test conditions. As shown in Fig. S1 (ESI<sup>†</sup>), the peak voltage outputs of ZnO NWs on unpoled PVDF (indicated by ZnO), only poled PVDF (indicated by PVDF), and ZnO NWs on poled PVDF but with the *c*-axis of the ZnO NWs in the same direction as the poling direction of PVDF (indicated by ZnO–PVDF) are 0.36 V, 0.27 V and 0.13 V, respectively. The results indicate that the output of the composite NG is the combined effect

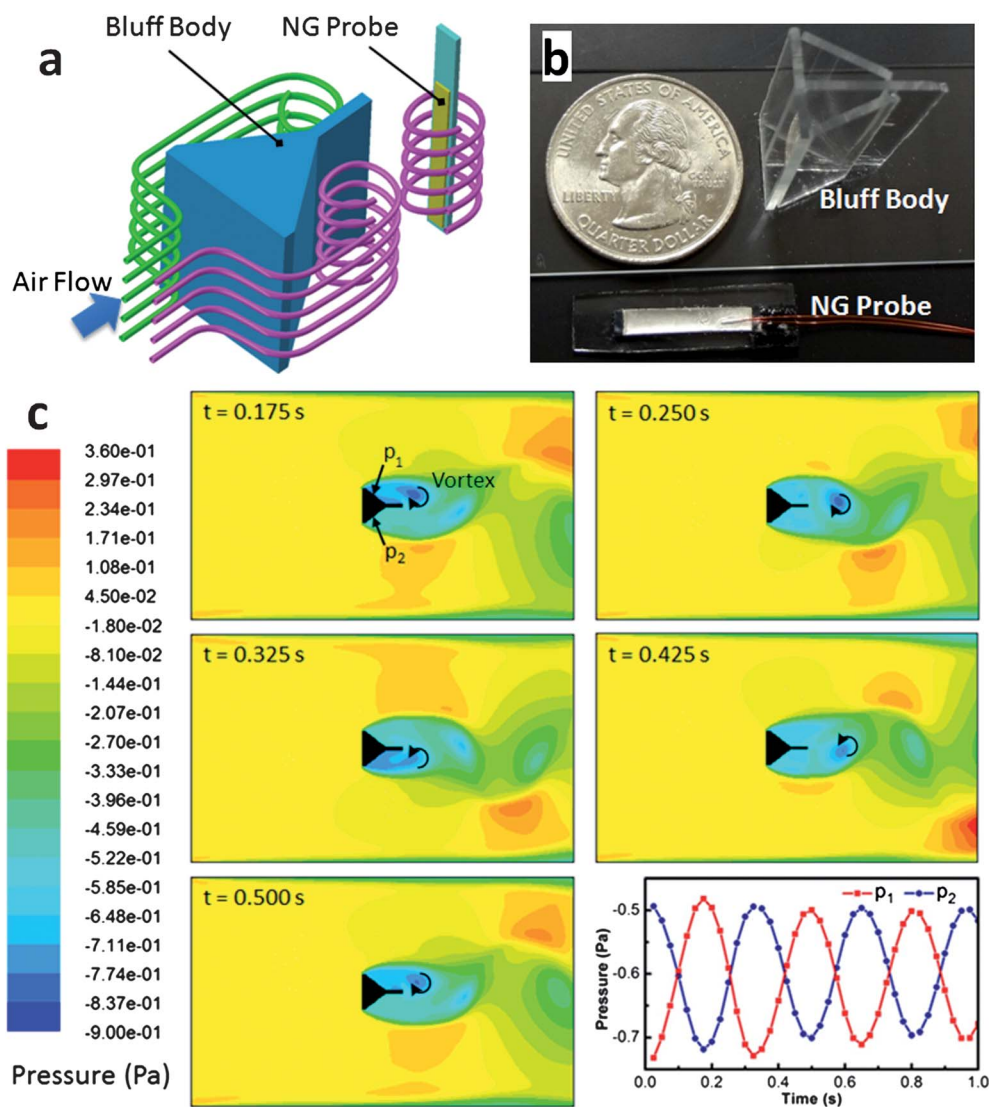


**Fig. 2** Schematic and simulation of the NG as an active sensor for detecting air flow. (a) Working principle of the vortex generation and capture. (b) Photo of the bluff body and the NG probe. (c) Transient pressure contours at different times, and curves of mean relative pressures on the two back faces.

of the ZnO NWs and the PVDF film. The ZnO NWs and the PVDF film are in series connection. Their output potentials add up or subtract depending on the polarization directions. Thus, the proposed structure is feasible for output enhancement.

### 3. NG-based vortex flow device (VFD)

The composite NG with high sensitivity and resolution is particularly suitable as an active sensor, such as a fluid sensor. When a fluid, which can be air, oil or water, flows through an obstacle or elbow pipe, inner turbulence can be generated with a change of the local flow speed or pressure. The change in local pressure can generate dynamic mechanical deformations, which can be measured through the voltage or current output of the NG. The sensor gives electric output without an external power source. This is the basic principle of the active fluid sensor.

With the NG as a vortex detector, an active VFD for super low air-flow velocity measurement is demonstrated, which can be as low as  $0.6 \text{ m s}^{-1}$ . Fig. 2a illustrates a schematic of the NG-based VFD. There are two main components in the system, the bluff body and the NG probe. The bluff body is designed as a triangle with a plate at its

end. It is fixed in a steady and weak air flow, with its front face vertical to the flow direction. The active sensor is made of a NG bonded on a glass strip substrate. It is placed in the wake of the bluff body. According to the Karman vortex street principle,<sup>17</sup> a row of vortices is generated on each side of the bluff body when the Reynolds number of the flow,  $Re$ , is in a certain range. The frequency of vortex shedding from the bluff body,  $f$ , depends on the input flow velocity,  $v$ , which is represented as<sup>17</sup>

$$v = \frac{fd}{St} \quad (1)$$

where  $St$  is the Strouhal number, a non-dimensional number related to  $Re$ ,  $d$  is the width of the bluff body.  $f$  is available by measuring the vortex induced local pressure variation with a NG probe. Thus, the flow velocity is obtained. A photo of the bluff body and NG probe is shown in Fig. 2b, and their dimensions are in Fig. S2 (ESI†).

With the proposed bluff body, vortices are visualized in Video S1 (ESI†). To understand the generation, distribution and strength of the vortices, computational fluidic dynamics is employed for vortex analysis. As shown in Fig. 2c, if we neglect the dimension and presence of the NG probe, a two-dimensional model of the bluff body is

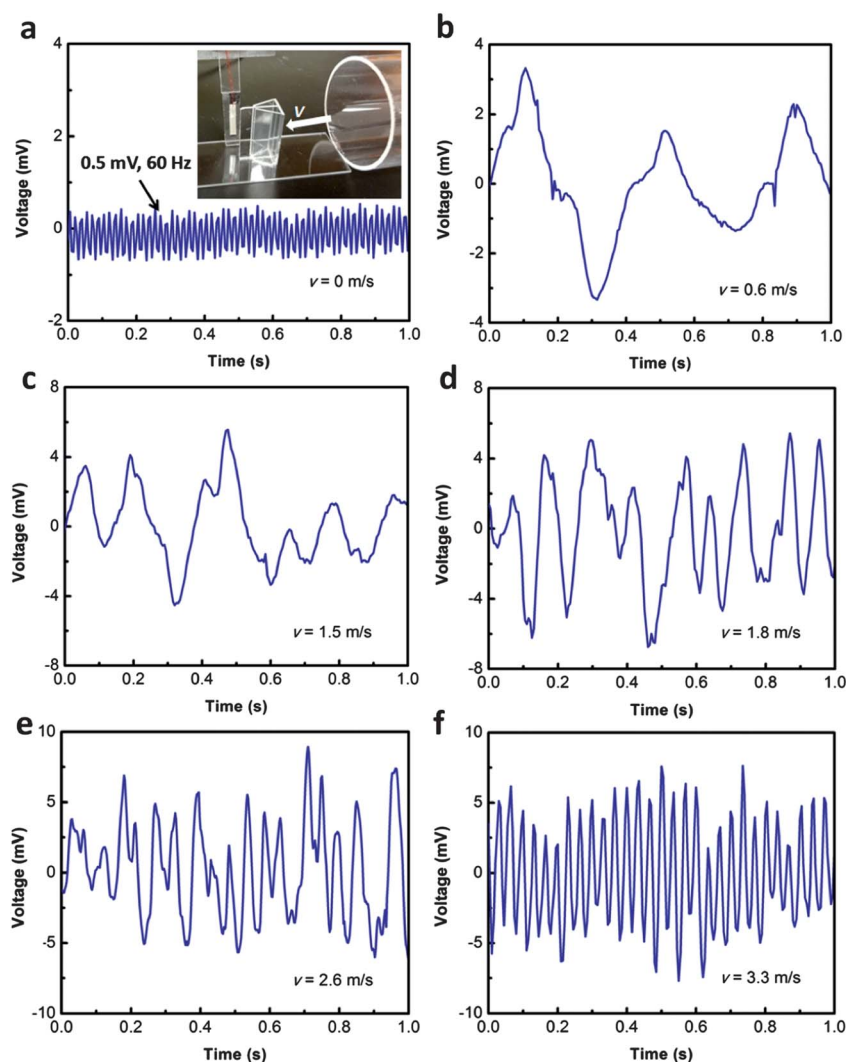


**Fig. 3** Voltage outputs of the NG under different air-flow velocities. (a)  $0 \text{ m s}^{-1}$ . The inset shows the VFD. (b)  $0.6 \text{ m s}^{-1}$ . (c)  $1.5 \text{ m s}^{-1}$ . (d)  $1.8 \text{ m s}^{-1}$ . (e)  $2.6 \text{ m s}^{-1}$ . (f)  $3.3 \text{ m s}^{-1}$ .

**Table 1** Velocity–frequency relationship

Velocity [ $\text{m s}^{-1}$ ]	0.6	1.5	1.8	2.6	3.3
Frequency [Hz]	2.9	6.8	8.9	18.9	29.7

built for the simulation. The model of the bluff body is placed in the center of a rectangular calculation region, whose dimension is  $134 \text{ mm} \times 80 \text{ mm}$ . The left- and right-hand side edges of the rectangular region are set as the velocity inlet at  $0.6 \text{ m s}^{-1}$  and the pressure outlet at atmosphere pressure, respectively. The unsteady flow induced by the bluff body is simulated with a time step of 25 ms, and the pressure distributions in the calculation region at different times are shown in Fig. 2c. The low pressure in a localised area is caused by the rotation of the vortex, so that the position of the vortex is indicated. It is observed that a vortex with clockwise direction is generated at the upper face of the bluff body at  $t = 0.175 \text{ s}$  and detaches from the bluff body gradually. The image at  $t = 0.25 \text{ s}$  shows the completely detached vortex. Then, an anticlockwise vortex is formed at the lower face at  $t = 0.325 \text{ s}$ , and subsequently it leaves the bluff body, as shown in the image at  $t = 0.425 \text{ s}$ . The above process is repeated periodically after  $t = 0.5 \text{ s}$ . The formation and detachment of vortices result in a pressure variation on the upper and lower triangle edges,  $p_1$  and  $p_2$ , are shown in the right bottom image in Fig. 2c, from which we can derive that the pressure variation is about 0.2 Pa and the frequency of vortex generation is around 3.25 Hz.

The vortices are detected with the NG as an active sensor. As shown in the inset photo in Fig. 3a, the bluff body is fixed in a calm

indoor environment. To acquire a controllable and steady air flow, compressed air is utilized to simulate the ambient wind. A tube with an inner diameter of 42 mm is placed ahead of the bluff body, with its outlet parallel to the front face of the bluff body. The other end of the tube is connected to the air source. The NG probe is placed in the wake of the bluff body vertically. By measuring the local pressure variation through the electrical output of the NG, the vortices are captured by the NG probe. To acquire the best vortex detection performance, the position of the NG probe is adjustable *via* a three-dimensional freedom platform. To calibrate the NG-based VFD, the flow velocity through the bluff body is measured with a commercial wind meter (Ambient Weather, HP816A). Fig. 3a shows the voltage output of the NG probe when input air-flow velocity is  $0 \text{ m s}^{-1}$ . The output with an amplitude of 0.5 mV and a frequency of 60 Hz is mainly from system interference, which is filtered out in the subsequent measurements. Fig. 3b–f show the outputs of the NG probe at different velocities from  $0.6 \text{ m s}^{-1}$ . Utilizing the fast Fourier transform (FFT) method, the frequencies of these outputs are analyzed and listed in Table 1. With the increase of the air-flow velocity, the vortex shedding frequency increases noticeably. The frequencies are 2.9, 6.8, 8.9, 18.9 and 29.7 Hz when air-flow velocities are 0.6, 1.5, 1.8, 2.6 and  $3.3 \text{ m s}^{-1}$ , respectively. By using the data fitting method, a cubic polynomial,  $v = 2.65 \times 10^{-4} f^3 - 1.59 \times 10^{-2} f^2 + 3.592 \times 10^{-1} f - 3.105 \times 10^{-1}$ , is obtained to depict the frequency–velocity relationship, which is important for the practical applications of this NG-based VFD. It should be noted that the flow velocity measured in this experiment is that through the bluff body, which is different from the inlet velocity in the above simulation. According to the fluid continuity equation, the air flow in the simulation is accelerated when

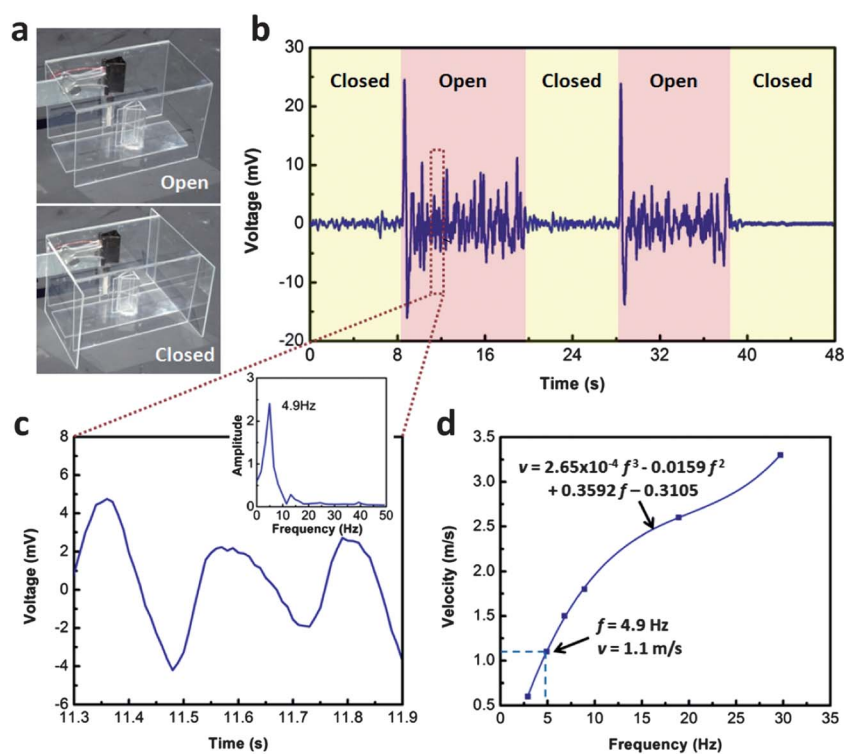


**Fig. 4** Ambient wind-speed measurement with the NG-based VFD. (a) Photos of the device with the wind passage open and closed. (b) Voltage output of the NG. (c) Magnified output curve from 11.3 s to 11.9 s. The inset shows the frequency spectrum of the output curve from 11.3 s to 11.9 s. (d) Frequency–velocity curve.

it flows through the bluff body. Thus, the velocity through the bluff body in the simulation is larger than  $0.6 \text{ m s}^{-1}$ , which leads to a slightly higher vortex shedding frequency of 3.25 Hz.

#### 4. Ambient wind-velocity measurement

The NG-based active VFD is utilized to measure the ambient wind-velocity. Since the direction of the wind in the outdoor environment is unsteady, the VFD is enclosed within glass to reduce the influence of direction variation. As shown in Fig. 4a, the outer glass and the bottom platform compose a rectangular wind passage, whose cross-sectional dimension is  $48 \text{ mm} \times 50.8 \text{ mm}$ . The inlet and outlet of the passage are parallel to the front face of the bluff body, so that the wind flows through the front face of the bluff body vertically. The passage can also be closed by covering the inlet and outlet with two pieces of glass. Therefore, the VFD has two working conditions, open or closed. The output under these conditions is shown in Fig. 4b and Video S2 (ESI<sup>†</sup>). When the passage is closed, the VFD output is less than 1 mV, which is from the system noise. The output voltage increases sharply and reaches a maximum value of 25 mV when the passage is opened suddenly, that is mainly because of the air-flow induced instantaneous pressure change around the NG probe. After the fierce fluctuation, the output voltage comes into a stable stage and fluctuates in the range of  $-10 \text{ mV}$  to  $10 \text{ mV}$ , which is the result of the motion of the vortices. When the passage is closed once again, the output returns to less than 1 mV. During the open stage, the wind velocity through the passage can be acquired by the FFT analysis of the output signal. The voltage output from 11.3 s to 11.9 s and its spectrum are shown in Fig. 4c and the inset, respectively. The main frequency at this time is about 4.9 Hz. As shown in Fig. 4d, by substituting the frequency into the previously obtained frequency-velocity curve, the transient wind-velocity is obtained as  $1.1 \text{ m s}^{-1}$ . Besides in ambient wind-velocity measurement, the NG-based active VFD can also be utilized in water flow and pipeline transmission monitoring, which should inspire research on self-powered wireless sensor networks for environment/infrastructure monitoring.

#### 5. Conclusions

In summary, we have demonstrated a high performance ZnO&PVDF composite nanogenerator for vortex capture and ambient wind-velocity detection. The composite structure design requires no extra fabrication processes, but greatly enhances the resolution and sensitivity of the NG, which makes the NG promising to be utilized as an active tiny signal sensor. The NG is successfully

utilized in vortex-based ambient wind-velocity detection in this study. It is demonstrated that the utilization of the NG broadens the lower measurement limit of vortex flow meters from  $6 \text{ m s}^{-1}$  to  $0.6 \text{ m s}^{-1}$ . The proposed NG-based sensor has wide applications in environment/infrastructure monitoring, such as gas-liquid flow and pipeline transmission measurements. Moreover, no battery or external power source needs to be used with the NG sensor. If we can use the energy harvested by the NG, self-powered wireless sensor networks can be built for detecting fluid flow.

#### Acknowledgements

This research was supported by MURI Airforce, BES DOE, National Nature Science Foundation for Distinguished Young Scholars (no. 50825502) and the Knowledge Innovation Program of Chinese Academy of Sciences (KJCX2-YW-M13). Rui Zhang is grateful for the fellowship from China Scholarship Council (CSC) (no. 2011602060).

#### References

- 1 N. S. Hudak and G. G. Amatucci, *J. Appl. Phys.*, 2008, **103**, 101301.
- 2 C. Knight, J. Davidson and S. Behrens, *Sensors*, 2008, **8**, 8037–8066.
- 3 B. J. Benson, B. J. Bond, M. P. Hamilton, R. K. Monson and R. Han, *Front. Ecol. Environ.*, 2010, **8**, 4.
- 4 Z. L. Wang and J. H. Song, *Science*, 2006, **312**, 5771.
- 5 X. D. Wang, J. H. Song, J. Liu and Z. L. Wang, *Science*, 2007, **316**, 5821.
- 6 S. N. Cha, S. M. Kim, H. J. Kim, J. Y. Ku, J. I. Sohn, Y. J. Park, B. G. Song, M. H. Jung, E. K. Lee, B. L. Choi, J. J. Park, Z. L. Wang, J. M. Kim and K. Kim, *Nano Lett.*, 2011, **11**, 12.
- 7 Y. Qin, X. D. Wang and Z. L. Wang, *Nature*, 2008, **451**, 809–813.
- 8 S. Xu, B. J. Hansen and Z. L. Wang, *Nat. Commun.*, 2010, **1**, 93.
- 9 G. Zhu, R. S. Yang, S. H. Wang and Z. L. Wang, *Nano Lett.*, 2010, **10**, 8.
- 10 Z. T. Li and Z. L. Wang, *Adv. Mater.*, 2011, **23**, 1.
- 11 M. Lee, C. Y. Chen, S. H. Wang, S. N. Cha, Y. J. Park, J. M. Kim, L. J. Chou and Z. L. Wang, *Adv. Mater.*, 2012, **24**, 13.
- 12 Y. F. Hu, C. Xu, Y. Zhang, L. Lin, R. L. Snyder and Z. L. Wang, *Adv. Mater.*, 2011, **23**, 35.
- 13 A. F. Yu, P. Jiang and Z. L. Wang, *Nano Energy*, 2012, **1**, 3.
- 14 Y. F. Hu, Y. Zhang, C. Xu, L. Lin, R. L. Snyder and Z. L. Wang, *Nano Lett.*, 2011, **11**, 6.
- 15 M. Lee, J. Bae, J. Lee, C. S. Lee, S. Hong and Z. L. Wang, *Energy Environ. Sci.*, 2011, **4**, 3359.
- 16 C. F. Pan, Z. T. Li, W. X. Guo, J. Zhu and Z. L. Wang, *Angew. Chem., Int. Ed.*, 2011, **50**, 47.
- 17 A. Venugopal, A. Agrawal and S. V. Prabhu, *Sens. Actuators, A*, 2011, **170**, 8–23.
- 18 L. Vayssieres, *Adv. Mater.*, 2003, **15**, 5.
- 19 Y. Qi and M. C. McAlpine, *Energy Environ. Sci.*, 2010, **3**, 1275–1285.